Analyst

Accepted Manuscript

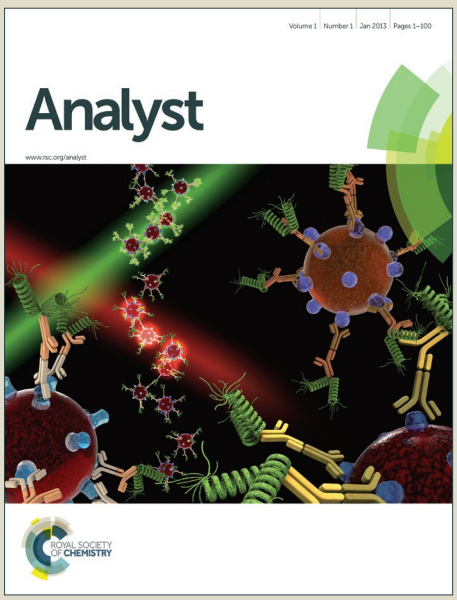

ROYAL SOCIETY OF CHEMISTRY

www.rsc.org/analyst

Cite this: DOI: 10.1039/c0xx00000x

www.rsc.org/xxxxxx

ARTICLE TYPE

A dual-mode colorimetric and fluorometric "light on" sensor for thiocyanate based on fluorescent carbon dots and unmodified gold nanoparticles

Dan Zhao, [a,b] Chuanxia Chen, [a,b] Lixia Lu, [a,b] FanYang, *[a] and Xiurong Yang*[a]

Received (in XXX, XXX) Xth XXXXXXXXX 20XX, Accepted Xth XXXXXXXXX 20XX
DOI: 10.1039/b000000x

Abstract: A novel, highly sensitive and selective dual-readout (colorimetric and fluorometric) sensor based on the fluorescent carbon dots (CDs) and unmodified gold nanoparticles (AuNPs) for the detection of thiocyanate (SCN^-) was proposed. Amino-functionalized CDs could be readily adsorbed onto the surface of citrate-stabilized AuNPs through Au-N interaction, leading to the aggregation of AuNPs and nonfluorescent off-state of CDs arising from the potential fluorescence resonance energy transfer (FRET). However, SCN^- had stronger affinity toward AuNPs and could compete with CDs to bind onto the surface of AuNPs in priority, which prevented the aggregation of AuNPs and fluorescence quenching of CDs. Correspondingly, both the colorimetric and fluorometric signals remained "light-on". The color of the sensing solution remained red and the fluorescence remained unquenched. A distinguishable change in the color was observed at a SCN^- concentration of 1 μM by naked eyes and a detection limit as low as 0.036 μM was obtained by virtue of fluorescence spectroscopy. Both colorimetric and fluorometric sensors exhibited excellent selectivity toward SCN^- over other common metallic ions and anions. In addition, such sensing assay featured simplicity, rapidity, cost-effectiveness and ease of operation without further modification. The accuracy and precision were evaluated based on the quantitative detection of SCN^- in tap water and saliva samples with satisfactory results.

Introduction

Thiocyanate anion (SCN^-), deriving from various sources such as industrial processes, e.g. fabric dyeing, hydrometallurgy, electroplating, and photofinishing, tabacoo smoke, diet and even car exhaust [1], poses potential threat to environment and human body owing to its cumulative effect. SCN^- could be converted to highly toxic cyanides through irradiation and chlorination, which results in serious environmental problems and health hazards.[2] Besides, SCN^- proves to be a small metabolite of CN^-, the accumulation of which arises from chronic tabacoo smoke exposure.[3] The level of SCN^- in body fluids can serve as an indicator to distinguish smokers from non-smokers. Notably, SCN^- can effectively block the uptake of iodide by the thyroid gland, leading to less formation of thyroxine and iodide deficiency, which is more serious for pregnant women and infant.[4] Exorbitantly high level of SCN^- gives rise to a higher risk of atherosclerosis, vertigo and unconsciousness.[5] All the abovementioned views underline the importance of SCN^- detection.

While several efficient methods for probing SCN^- exist, including spectrophotometry,[6] ion chromatography,[7] surface-enhanced Raman scattering (SERS),[8] electrophoresis,[9] electrochemistry[10] and fluorimetry,[11,12] the involvement of tedious procedures, sophisticated manipulation and unpleasant or harmful reagents usually limits their application. Accordingly, simple, reliable and straightforward methods are still in high demand for the rapid and sensitive determination of SCN^-.

With the rapid development of nanotechnology, research interests to develop efficient methods by virtue of nanoscaled materials have been growing unabated. Optical sensing assays with colorimetric and fluorometric dual modes have sparked significant excitement due to the fact that they can offer more than one kind of output signal simply and rapidly, thus making the detection results more convincing. [13, 14] Due to the strong distance-dependent property and extremely high extinction coefficient of gold nanopraticles (AuNPs), ongoing efforts have been made to explore facile colorimetric sensors utilizing AuNPs as an ideal colorimetric indicator for the detection of SCN^-.[15-17] The colorimetric detection could be realized by the unique and distinct color variation during aggregation of AuNPs (red to blue) or redispersion of the aggregated AuNPs (blue to red). Correspondingly, a significant shift of the surface plasmon resonance (SPR) absorbance band to a longer wavelength or *vice versa* could be also observed.[18] Meanwhile, fluorometric methods relying on fluorescence resonance energy transfer (FRET), which could occur when the emission spectrum of the donor is appreciably overlapped with the absorption spectrum of the acceptor to some extent, have become a hot topic in the field of fluorescent biosensor.[19] By taking advantage of the strong quenching ability of AuNPs, various FRET-based fluorescence

sensors have been established for probing ions,[20] small molecules[21, 22] and proteins,[23] where a wealth of organic dyes and quantum dots (QDs) such as rhodamine B,[24] rhodamin 6G,[25] fluorescein,[26] CdTe QDs[27] and carbon dots (CDs)[28] have proven to be efficient energy donors (fluorescence reporters). Recently, Ma and coworkers devised a simple and ultrasensitive turn-on fluorometric sensor for SCN^- using fluorescein as an energy donor.[29] To the best of our knowledge, all previous sensors have been focused on single readout, which stimulates us to develop a colorimetric and fluorimetric dual-readout sensor for simple and rapid SCN^- sensing. This kind of probe possesses two different signals for target, thus increasing the sensing diversity. The dual-readout sensing system combines the high sensitivity of fluorescence assay and the convenience and low cost of visual assay. More importantly, the simultaneous optical signal changes can help to enhance the accuracy for SCN^- detection.

Herein, we proposed a new, convenient and dual-mode "light-on" sensor with colorimetric and fluorometric readout for monitoring the concentration of SCN^-. The amino-functionalized CDs could readily bind to the surface of citrate-stabilized AuNPs through Au-N interaction, thus inducing the aggregation of AuNPs and fluorescence quenching of CDs due to the potential FRET. The detection of SCN^- was based on the preferential binding of SCN^- toward the surface of AuNPs due to the stronger Au-S covalent bond. Once the AuNPs were pretreated with SCN^-, the interaction between AuNPs and CDs was prevented. As a result, the colorimetric and fluorometric signals were effectively switched on. This dual-mode sensing platform can not only enable the visualization of SCN^- simply with naked eyes, but also provide a reliable fluorescence assay with simplicity and rapidity.

Experimental

Chemicals and apparatus

Hydrogen tetrachloroaurate (Ⅲ) trihydrate ($HAuCl_4 \cdot 3H_2O$), L-histidine and potassium thiocyanate (KSCN) were purchased from Sigma-Aldrich (USA). Other inorganic salts were bought from Beijing Chemical Reagent Co. (China). Phosphate buffer solutions (PBS) with various pH values were obtained by mixing 100 mM Na_2HPO_4 and NaH_2PO_4 stock solution with different ratios and diluted to the concentration demanded. All of these chemicals were at least of analytical reagent grade and used without further purification. The ultrapure water used throughout all the experiments was purified through a Millipore system (Millipore, USA).

UV-vis and fluorescence spectra were recorded with a Cary 50 UV-vis spectrophotometer (Varian) and a Hitachi F-4600 spectrofluorometer (Tokyo), respectively. Photographs were taken with a commercial digital camera. The X-ray photoelectron spectroscopy (XPS) samples on highly cleaned silicon wafers were analyzed by Thermo ESCALAB MKII spectrometer (VG Scientific) with Al Kα X-ray radiation as X-ray source for excitation. Transmission electron microscopy (TEM) and high resolution TEM (HRTEM) measurements were carried out on a Tecnai G2 F20 (FEI) with an accelerating voltage of 200 kV. The samples were prepared by applying a droplet of the diluted solution to carbon-coated copper grids and dried naturally. Dynamic light scattering (DLS) experiments were performed on a Malvern Zetasizer instrument (Malvern). Fourier transform infrared (FTIR) data were acquired with a VERTEX 70 Fourier transform infrared spectrometer (Bruker).

Synthesis of citrate-stabilized AuNPs and amino-functionalized CDs

AuNPs were prepared by the citrate reduction of $HAuCl_4$ according to the well-known Turkevich-Frens method.[30] All glasswares used in the preparation were soaked in aqua regia and rinsed thoroughly with ultrapure water before use. Briefly, 100 mL of 1 mM $HAuCl_4$ solution was heated to boiling under vigorous stirring. Then 10 mL of 38.8 mM trisodium citrate was quickly injected. This mixture was allowed to stir for another 15 min. The resulting wine-red solution was cooled down to room temperature and stored at 4 ºC.

Herein, fluorescent CDs were prepared by one-pot hydrothermal treatment of histidine. [31] Briefly, 2.5 g of histidine was dissolved in 25 mL of 0.5 mM NaOH. Then the solution was transferred to a 50 mL Teflon equipped stainless steel autoclave and heated at 180 ºC for 12 h. The dark yellow solution was dialyzed against ultra-pure water through dialysis membrane (MWCO of 1000) for 24 h. The as-obtained purified CDs aqueous solution was stored at 4 ºC for subsequent use and characterization.

Assay procedure for thiocyanate determination

Typically, 150 μL of as-prepared AuNPs, 280 μL of PBS buffer solution (pH 7.0, 10 mM) and 40 μL of various concentrations of SCN^- solution were sequentially added to a series of centrifuge tubes. After homogenous mixing and stabilizing for 5 min, 30 μL of CDs were introduced to the tubes and further incubated for 8 min. Then, the mixture was transferred for UV-vis scanning and fluorescence measurements at ambient temperature.

Thiocyanate detection in real samples

For the analysis of water samples, 0.1 mM EDTA was added to eliminate the potential interference of metallic ions. The tap water was analyzed without further treatment. Saliva samples of healthy smokers and non-smokers were collected more than 1 h after meal, and centrifuged at 7000 g for 30 min after diluting with ultrapure water. In order to fit the standard calibration curve, it was worth mentioning that the smoker and non-smoker's saliva were diluted by 1000 and 200 times, respectively. A standard addition method was employed to validate the method. The water and saliva samples were spiked with different concentrations of SCN^- and used for colorimetric and fluorimetric assay.

Results and discussion

Characterizations of AuNPs and CDs

The optical properties of the as-prepared nanoparticles were investigated by UV-vis absorption spectra and fluorescence spectra. As shown in Fig. 1, AuNPs displayed a prominent SPR absorption at 520 nm. The particle concentration was estimated to be about 11 nM according to Beer's law using an extinction coefficient of *ca.* $2.7\times10^8\ M^{-1}\ cm^{-1}$ at 520 nm. [32]

The CDs aqueous solution emitted obvious blue fluorescence under UV light (365 nm) while appearing yellow transparent under daylight (inset of Fig. 1). As shown in Fig.1, the UV-vis

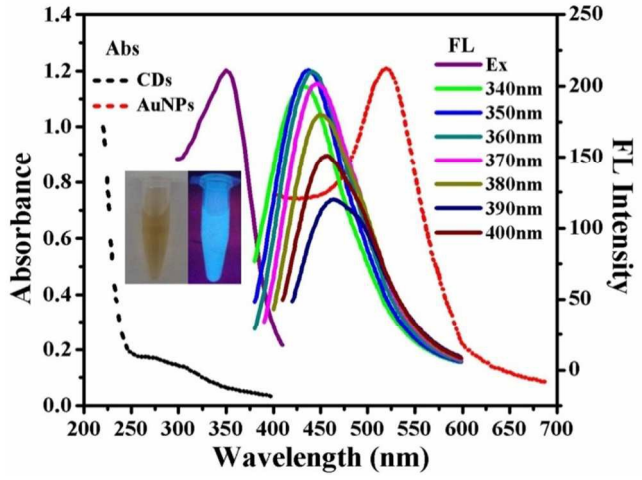

Fig. 1. The UV-vis absorption spectra of CDs and AuNPs; the excitation spectrum and emission spectra of CDs. Inset shows the photograph of the CDs under visible light (left) and 365 nm UV light (right), respectively.

spectrum showed a broad peak at about 280 nm, which was possibly assigned to the π→π* transition of nanocarbon.[33] The CDs exhibited an excitation-dependent emission behavior similar to that of previous report on CDs, which might be due to the optical selection of differently sized CDs and their surface defects.[34] Along with the excitation wavelengths varying from 340 nm to 400 nm, the emission peaks demonstrated a gradual red-shift from 435 nm to 460 nm. When excited at 350 nm, the CDs exhibited the strongest emission located at 438 nm.

The surface composition and elemental analysis of the fluorescent CDs were characterized by XPS techniques. The full scan XPS spectrum demonstrated in Fig. S1 exhibited three major peaks at 284.55, 399.26 and 530.66 eV corresponding to C 1s, N 1s and O 1s, respectively. Another peak at 1072 eV attributed to Na 1s which may come from NaOH was also observed. As revealed in the high resolution spectrum of C 1s (Fig. S2A), there existed two devonvoluted peaks with binding energies of 284.6 and 288.1 eV, which demonstrated the presence of C–C and C=N/C=O functional groups. The two peaks at 399.1 and 400.4 eV in N 1s pectrum (Fig. S2B) were assigned to C–N–C and N–H, respectively. Another peak at 407 eV was also observed, which indicated the presence of $–NO_3$. The XPS results showed strong signals from both amine-N and doping N atoms, which was further verified by the FTIR data (Fig. S3). The broad bands centered at 3380, 3248, and 3125 cm^{-1} suggested the existence of –OH, $–NH_2$ and $–NH_3^+$, respectively. In addition, the stretching vibrations of amide I, C=O, amide II, N-H and amide III, C-N could be observed at 1610, 1497, and 1392 cm^{-1}, respectively.

General mechanism for the detection of thiocyanate

In the present work, we proposed a one-pot green route to prepare blue-emitting CDs using histidine as nitrogen-doped carbon source and adopted the synthesized CDs as a fluorometric reporter for the detection of SCN^- (Scheme 1). AuNPs play a dual role in this sensing system. Firstly, the AuNPs behave as colorimetric indicator enabling the colorimetric analysis. Secondly, the AuNPs serve as fluorescence quencher, which has been proved to possess an extraordinary quenching efficiency in a broad range of wavelengths.[35, 36] As can be obviously seen from

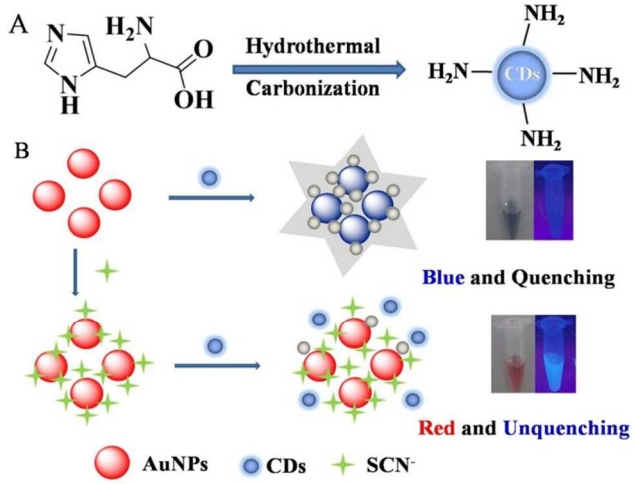

Scheme 1. The schematic illustration of (A) the synthetic process of amino-functionalized CDs and (B) the mechanism of the dual-readout nanosensor for SCN^- detection.

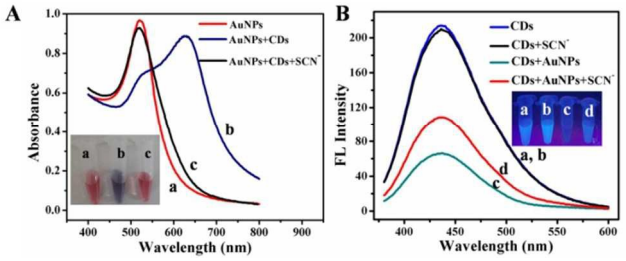

Fig. 2. (A) UV-vis absorption of AuNPs (a), AuNPs + CDs (b) and AuNPs + CDs+ SCN^- (c). (B) Fluorescence emission spectra of the CDs (a), CDs + SCN^- (b), CDs + AuNPs (c) and CDs + AuNPs + SCN^- (d). Inset shows the corresponding color changes.

Fig. 1, the emission spectrum of CDs overlaps the absorption spectrum of AuNPs to some extent, indicating that efficient FRET may occur from CDs to AuNPs. The amino-functionalized CDs can be readily adsorbed on the surface of citrate-AuNPs through Au-N interaction to form CDs-AuNPs ensemble, resulting in the aggregation of AuNPs and the fluorescence quenching of the CDs. In fact, the affinity between –SCN and AuNPs is comparable to that of –SH and AuNPs.[37] Accordingly, SCN^- competes with CDs for binding on the surface of AuNPs in priority, thus protecting AuNPs from aggregation. Simultaneously, the fluorescence of CDs remained unquenched. Based on this feature, excellent analytical performance for this dual-mode sensor for SCN^- could be anticipated.

Characteristics of the dual-readout sensor

To get more insight into the designed sensor, the TEM, DLS, UV-vis and fluorescence measurements were carried out. The dispersed AuNPs exhibited wine-red color with a strong absorption peak at 520 nm (inset a and curve a, Fig. 2A). As expected, AuNPs aggregated immediately upon the addition of CDs, manifested by the dramatic decrease in the absorbance at 520 nm and the concomitant red-shift of the SPR absorption to 630 nm, along with a blue solution being observed (inset b and curve b, Fig. 2A). If SCN^- was mixed with AuNPs in advance and then CDs were added, the aggregation of AuNPs was significantly attenuated due to the strong Au-S covalent bond

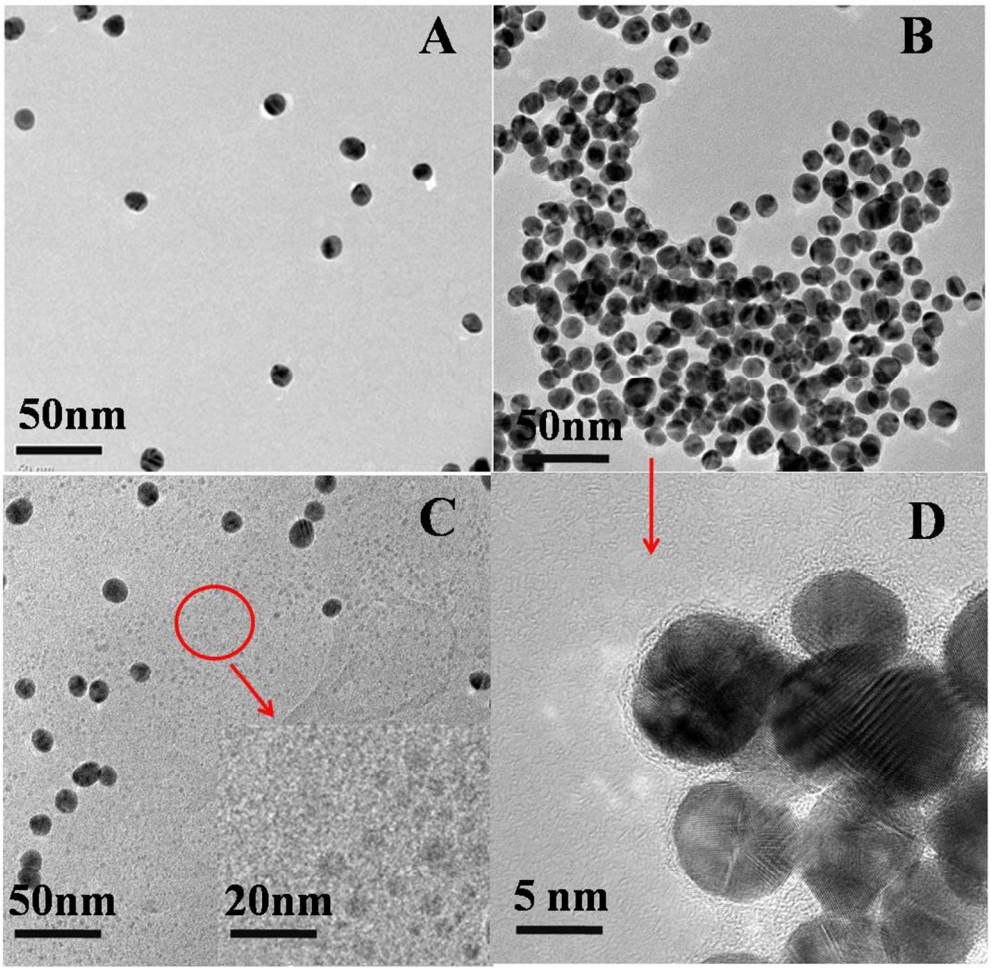

Fig. 3. TEM images of dispersed AuNPs (A), aggregated AuNPs induced by CDs in the absence of SCN^- (B), the dispersed AuNPs in the presence of CDs and SCN^- (C) and HRTEM image of aggregated AuNPs induced by CDs (D).

(inset c and curve c, Fig. 2A). As can be seen from the TEM image in Fig. 3A, the as-prepared AuNPs were monodisperse, spherical and regular in shape with an average diameter of about 13 nm. Besides, the CDs-stimulated aggregation of AuNPs was further confirmed by the TEM observations (Fig. 3B). HRTEM image (Fig. 3D) displays a compact "shell" on the surface of AuNPs, which demonstrated the presence of adsorbed CDs. Moreover, the well-dispersed AuNPs in TEM image of Fig. 3C verified the effective protection of SCN^- toward the AuNPs probe. Obviously, the small particles in Fig. 3C indicated the existence of dispersed CDs. Further evidence could be obtained by comparing the DLS data of corresponding solutions (Fig. S4). The DLS data showed that the average hydrodynamic diameter of well dispersed AuNPs was 12.5 nm, while that of the CDs-induced aggregated AuNPs increased to 65.8 nm. However, when SCN^- was added into the sensing system in advance, the average diameter of AuNPs was about 15.6 nm, which confirmed that SCN^- could effectively prevent the aggregation induced by CDs.

In order to further confirm the potential FRET, we investigated the effect of AuNPs concentrations on the assay system. Mixing of CDs and AuNPs could form donor-acceptor assembly through Au-N interaction and the fluorescence of CDs was promptly quenched (Fig. S5A). As shown in Fig. S5A, the fluorescence gradually decreased with an increasing concentration of AuNPs. A diagram plotting F_0/F as a function of [AuNPs] was shown in the inset of Fig. S5B. The Stern-Volmer equation was fitted as:

$F_0/F = 0.535 \times [Q]\ (nM) + 1\ (R^2=0.991)$

where F_0 and F denoted the fluorescence intensity of CDs before and after the quencher addition. According to the slope of the linear plot, the quenching constant (K_{SV}) was calculated to be $0.535 \times 10^9\ M^{-1}$, signifying high quenching efficiency.[38] Additionally, this large quenching constant ensured a stable off-state in the following sensitive turn-on quantitative analysis for SCN^-.

Fig. 2B depicts the competitive effect between SCN^- and CDs. The fluorescence emission spectrum of the mixture of CDs and SCN^- (curve b, Fig. 2B) was almost identical to that of the individual CDs (curve a, Fig. 2B), which unambiguously illustrated that there was no obvious interaction between SCN^- and CDs. When AuNPs were mixed with CDs, the fluorescence was significantly decreased through FRET (curve c, Fig. 2B). However, in the presence of SCN^-, SCN^- could preferentially bind to the surface of AuNPs, which prevented the interaction between CDs and AuNPs, thus reduced the FRET effect, leading to the increase of the fluorescence intensity (curve d, Fig. 2B). The evolution of the fluorescence under UV light also demonstrated

the feasibility of the strategy (the inset of Figure 2B). On the basis of the abovementioned results, a fluorometric "light-on" sensor for the determination of SCN^- was proposed.

Optimization of the experimental conditions for SCN^- detection

To obtain better performance, the sensing conditions, including buffer pH, the volume of CDs and incubation time were optimized. The fluorescence enhanced efficiency was defined as $(F-F_0)/F_0$, where F and F_0 corresponded to the fluorescence intensity in the presence and absence of SCN^-, respectively. Fig. S6A unveils that the capability of CDs to aggregate AuNPsreduces with the decrease of buffer pH values. It can be observed that the value of A_{630}/A_{520} in the presence and absence of SCN^- both stepwise decreased with the pH ranging from 5.8 to 8.2. In addition, satisfactory results for colorimetric and fluorometric response emerged at pH=7.0 (Fig. S6B), where the difference of A_{630}/A_{520} ($\Delta A_{630}/A_{520}$) in the presence and absence of SCN^- reached the maximum value. Therefore, pH 7.0 was chosen as the detection pH in the sbusequenct experiments. It should be noted that the volume of CDs played an improtant role in this study. The absorbance ratio A_{630}/A_{520} increased with increasing volume of CDs, revealing that the addition of CDs faciliated AuNPs aggregation. However, excessive CDs obstructed the interaction between SCN^- and AuNPs, resuting in the decrease of the sensitivity. The results in Fig. S7 showed that the maximum response of SCN^- ($\Delta A_{630}/A_{520}$) was observed when the volume of CDs was 30 μL. In additon, CDs-AuNPs system under this condition gave an ideal nonfluorescent off-state for the subsequent analysis. So 30 μL CDs was selected for further investigations. A suitable incubation time of AuNPs and SCN^- was expected to yield a satisfactory detection result. As shown in Fig. S8, the colorimetric and fluorometric signals increased gradually as the incubation time prolonged and leveled off after 6 min. To summarise, pH 7.0, 30 μL of CDs and 6 min served as the optimal conditions in this proposed assay.

Colorimetric readout for SCN^- detection

Under the optimized conditions, sensing solutions in the presence of various concentrations of SCN^- were observed by naked eyes or subjected to UV-vis scanning. Fig. 4A shows that the color of the sensing system gradually changes from blue to red with the increase of SCN^- concentration. When the concentration of SCN^- was 1 μM, an apparent color change could be differentiated from the intitial solution by naked eyes. As manifested in Fig. 4B, the increase of SCN^- concentration resulted in the systematic increase of the absorbance at 520 nm and the decrease of the absorbance at 630 nm, which was consistent with the color change displayed in Fig. 3A, indicating the effective protection of SCN^- toward the AuNPs probe. A linear relationship between A_{630}/A_{520} and the SCN^- concentration in the range of 0.2-2 μM was obtained with a correlation coefficient of 0.991 (the inset in Fig. 4C). The limit of detection (LOD) was estimated to be 0.14 μM at a signal-to-noise ratio of 3. These analytical parameters were favorably comparable or even better than those previously reported colorimetric methods listed in Table S1.

In addition to SCN^-, a number of anions were also tested in the colorimetric system. Apart from SCN^-, it was found that the aggregation of AuNPs was retarded by other five anions (Br^-, S^{2-}, $S_2O_3^{2-}$, I^- and CN^-) (Fig. S9). However, the interference from CN^-

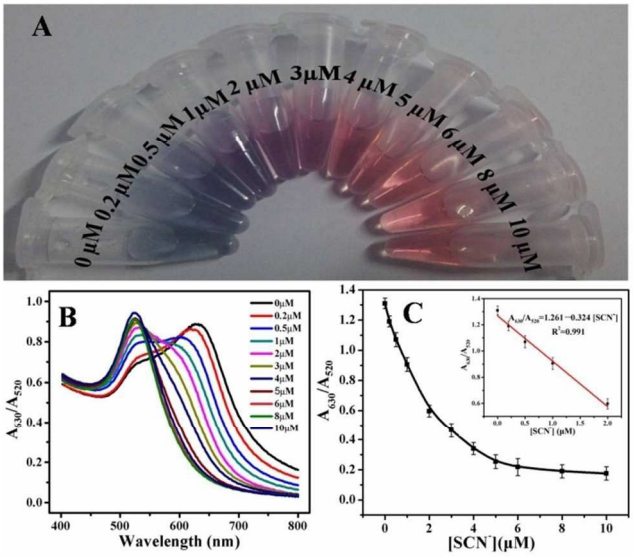

Fig. 4. (A) Photographs of colorimetric responses toward various concentrations of SCN^-. (B) UV-vis absorption spectra of the proposed assay in the presence of different amounts of SCN^-. (C) Relationship between the A_{630}/A_{520} ratio and the concentration of SCN^- (Inset shows the linear calibration plot corresponding to the SCN^- concentration).

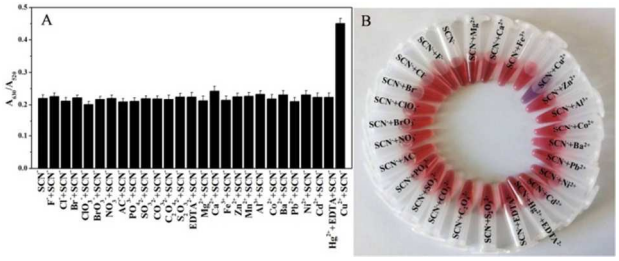

Fig. 5. (A) Interference study of the sensor in the presence of a mixture of SCN^- and another foreign ion. (B) shows the corresponding digital images. Concentrations: 5 μM for SCN^- , 10 μM for Br^- and Fe^{3+}, and 50 μM for other ions.

was not fatal to our proposed sensor. CN^- occurred rarely in nature and was barely detected in water and saliva samples. The interference of Br^- and $S_2O_3^{2-}$ could be ignored when their concentrations were below 10 μM and 2 μM, respectively. In addition, the response of S^{2-} and I^- could be eliminated in the presence of masking agents such as $S_2O_8^{2-}/Pb^{2+}$ (Fig. S10), which facilitated the selective detection of SCN^-. Besides the anions, various metallic ions were also tested in the mixture with SCN^- for colorimetric responses. As elucidated in Fig. 5A, none of them other than Cu^{2+} and Hg^{2+} could exert noticeable interference to the SCN^- detection results. The reason for the interference from Cu^{2+} may lie in the reduction of Cu^{2+} by SCN^- to Cu^+ and the subsequent formation of mixed-valence species due to the high stability constant.[39] However, SCN^- could not coexist with Cu^{2+}, so the interference from Cu^{2+} need not to be considered. As reported [40], chemicals containing more than one amino group were effective as bridge molecules for the AuNPs-based sensing of Hg^{2+}. The reaction between Hg^{2+} and the amino group is the main basis of the bridge effect for the aggregation of AuNPs. Therefore, in the presence of Hg^{2+}, amino-CDs could serve as a bridge molecule to induce the aggregation of AuNPs. The bridge effect between the amino group and Hg^{2+} other than the

interaction between CDs and AuNPs was the driving force of the aggregation of AuNPs. As a result, Hg^{2+} dramatically influenced the colorimetric response (Fig. S11A). However, the interference from Hg^{2+} could be eliminated when EDTA was used as a making reagent (Fig. S11A). In addition, remarkable selectivity could also be acquired by naked-eye observation (Fig. 5B). All the results above demonstrated the applicability of this proposed assay for the colorimetric probing of SCN^- in the presence of other foreign substances.

Fluorometric readout for SCN^- detection

As expected, the suppression of the FRET effect due to the preferential binding affinity of SCN^- to AuNPs can be validated by the fluorescence "light-on" of the sensing system. Fig. 6A displayed the gradual increase of fluorescence response at 438 nm of our proposed assay when the concentration of SCN^- increased. It was clear that $(F-F_0)/F_0$ exhibited a linear response to the SCN^- concentration in the range of 0.1-1.6 μM (Fig. 6B). Compared with other previous fluorometric sensors listed in Table S1, a competitive LOD of 0.036 μM (3σ) was achieved. A relative standard deviation (RSD) of 2.49% was obtained by repetitive measurements of 3 μM SCN^- for 6 times, suggesting the excellent reproducibility of the proposed sensor.

To evaluate the selectivity of this fluorescent probe, the fluorimetric responses from other foreign substances were investigated. Among the tested ions, the presence of Hg^{2+} could lead to significant fluorescence enhancement. Fortunately, the problem could be solved by spiking EDTA into the sensing system (Fig. S11B). In addtion, 50 μM of Na^+, K^+, Mn^{2+}, Zn^{2+}, Pb^{2+}, Co^{2+}, Ca^{2+}, Mg^{2+}, EDTA, F^-, Cl^-, Br^-, S^{2-}, PO_4^{3-}, NO_3^-, SO_4^{2-}, CO_3^{2-} and SO_3^{2-} and 10 μM of Br^- and Fe^{3+} did not interfere with the detection (Fig. 7). The reason was that these substances could not form a stronger bond than that beween CDs and AuNPs. These results further indicated that the proposed sensing system could serve as a "turn-on" fluorometric sensor for label-free detection of SCN^- with high sensitivity and selectivity.

Application in real samples

To further validate the feasibility of the proposed nanosensor in practical applications, we applied the sensor to detect SCN^- in saliva and tap water samples colorimetrically and fluorometrically. It was found that SCN^- concentration in tap water was too low to be detected by our sensor. The standard additon experiments with three spiked levels of SCN^- were carried out and the results were shown in Table 1. Satisfactory recoveries between 89.7% and 102% with RSDs from 1.97% to 3.56% were obtained. Considering that the saliva samples of non-smoker and smoker were 200 and 1000 times diluted, the obtained value should be mutipled by 200 and 1000, respectively. Obviously, the level of SCN^- in smokers' saliva was much higher than that in non-smokers' saliva. Our detected concentrations were consistent with the previously reported statistic data and that by other sensors.[41] These results indicated that this dual-mode sensor can be applied to the detection of SCN^- in tap water and saliva samples with high sensivity and selectivity.

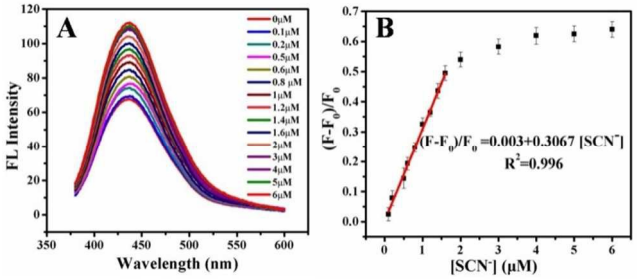

Fig. 6. (A) The fluorescence emission spectra of CDs in the presence of different concentrations of SCN^-. (B) The fluorescence enhancement efficiency as a function of SCN^- concentration.

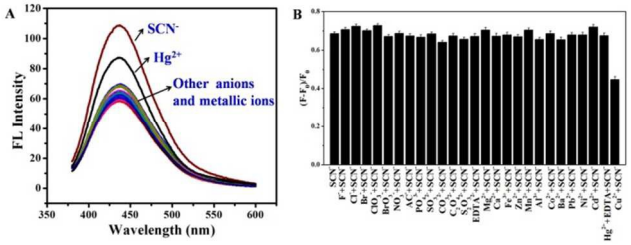

Fig. 7. (A) The fluorescence emission spectra of the proposed assay in the presence of SCN^- or other foreign anions and metallic ions. (B) Interference study of the sensor in the presence of a mixture of SCN^- and other foreign ion. Concentrations: 5 μM for SCN^-, 10 μM for Br^- and Fe^{3+}, and 50 μM for other ions.

Table 1. The application of the proposed nanosensor for determination of SCN^- in tap water and human saliva samples.

Samples	Measure Mode	Found in sapmles (μM)	Added (μM)	Total found (μM)	Recovery (%)	RSD (n=3, %)
Tap Water	Colorimetry	—	0.5	0.501	100.2	3.12
			1	0.897	89.7	2.98
			1.5	1.42	94.6	3.47
	Fluorimetry	—	0.5	0.489	97.8	2.64
			1	1.02	102	2.13
			1.5	1.45	96.6	2.97
Non-smoker saliva [a]	Colorimetry	0.546	1	1.56	101.4	2.65
	Fluorimetry	0.568	1	1.55	98.2	1.97
Smoker saliva [b]	Colorimetry	0.724	1	1.66	93.7	3.56
	Fluorimetry	0.743	1	1.75	100.7	2.39

[a] diluted by 200 times, [b] diluted by 1000 times.

Conclusions

In summary, a simple, sensitive and reliable dual-mode "light on" sensor for SCN^- has been fabricated in this work. Due to the stronger Au-S covalent interaction, SCN^- could compete with CDs to bind onto the surface of AuNPs, and as a consequence, the color of the sensing solution remains red and the fluorescence of CDs remains unquenched simultaneously. This dual-readout sensor allows detection of SCN^- in tap water and human saliva samples with satisfactory results. This simple assay provides a reliable option to detect SCN^- with high sensitivity and selectivity. As far as we know, this is the first time to propose a sensor for SCN^- based on CDs and AuNPs with two different responses. Therefore, given its simplicity, flexibility and easy operation, our proposed strategy may give a new sight for discriminative detection of other analytes with multiple optical signals.

Acknowledgements

This work was supported by the National Natural Science Foundation of China (No. 21435005 and No. 21175124).

Notes and references

[a] *State Key Laboratory of Electroanalytical Chemistry, Changchun Institute of Applied Chemistry, Chinese Academy of Sciences, Changchun, Jilin 130022, China Fax:* +86 431 85689278*; Tel:* +86 431 85262056; E-mail: xryang@ciac.ac.cn

[b] *University of Chinese Academy of Sciences, Beijing 100049, China.*

† Electronic Supplementary Information (ESI) available: Fig.S1-S11 and Table S1. See DOI: 10.1039/b000000x/

1 Y. Zhang, H. Wang and R. H. Yang, *Sensors*, 2007, **7**, 410.

2 R. M. Naik, B. Kumar and A. Asthana, *Spectrochim. Acta A*, 2010, **75**, 1152.

3 M. T. Ashby, A. C. Carlson and M. J. Scott, *J. Am. Chem. Soc.*, 2004, **126**, 15976.

4 S. E. Chemaly, M. Salathe, S. Baier, G. E. Conner and R. Forteza, *Am. J. Respir. Crit. Care Med.*, 2003, **167**, 425.

5 L. Wu, Z. Y. Wang, S. F. Zong and Y. P. Cui, *Biosens. Bioelectron.*, 2014, **62**, 13.

6 J. Zhang, Y. Yuan, X. W. Xu, X. L. Wang and X. R. Yang, *ACS Appl. Mater. Interfaces*, 2011, **3**, 4092.

7 R. A. Niemann and D. L. Anderson, *J. Chromatogr. A*, 2008,**1200**, 193.

8 B. A. Logue, D. M. Hinkens, S. I. Baskin and G. A. Rockwood, *Crit. Rev. Anal. Chem.*, 2010, **40**, 122.

9 Z. Q. Xu, T. Doi, A. R. Timerbaev and T. Hirokawa, *Talanta*, 2008, **77**, 278.

10 M. Arvand, M. A. Zanjanchi and L. Heydari, *Sens. Actuators B*, 2007, **122**, 301.

11 B. Gonga and G. Q. Gong, *Anal. Chim. Acta*, 1999, **394**, 218.

12 A. Banerjee, A. Sahana, S. Lohar, I. Hauli, S. K. Mukhopadhyay, D. A. Safin, M. G. Babashkina, M. Bolte, Y. Garcia and D. Das, *Chem. Commun.*, 2013, **49**, 2527.

13 D. Zhao, C.X. Chen, L.X. Lu, F. Yang and X.R. Yang, *Sens. Actuators B*, 2015, **215**,437.

14 Y. Ling, Z. F. Gao, Q. Zhou, N. B. Li and H. Q. Luo, *Anal. Chem.*, 2015, **87**,1575.

15 Z.Y. Zhang, J. Zhang, C. Qu, D. Pan, Z. Chen and L. Chen, *Analyst*, 2012, **137**, 2682.

16 H. H. Deng, C. L. Wu, A. L. Liu, G. W. Li, W. Chen and X. H. Lin, *Sens. Actuators B*, 2014, **191**, 479.

17 J. Zhang, C. Yang, X. L. Wang and X. R. Yang, *Anal. Bioanal. Chem.*, 2012, **403**, 1971.

18 D. B. Liu, Z. Wang and X. Y. Jiang, *Nanoscale*, 2011, **3**, 1421.

19 B. Tang, L.H. Cao, K. H. Xu, L. H. Zhuo, J. C. Ge, Q. L. Li and L.J. Yu, *Chem. Eur. J.*, 2008, **14**, 3637.

20 J. L. Chen, A. F. Zheng, A. H. Chen, Y. C. Gao, C. Y. He, X. M. Kai, G. H. Wu and Y. C. Chen, *Anal. Chim. Acta*, 2007, **599**, 134.

21 Y. P. Shi, H. Zhang, Z. F. Yue, Z. M. Zhang, K. S. Teng, M. J. Li, C. Q. Yi and M. S. Yang, *Nanotechnology* , 2013, **24**, 375501.

22 W. P. Wang, Y. C. Lu, H. Huang, A. J. Wang, J. R. Chen and J. J. Feng, *Biosens. Bioelectro.*, 2015, **64**, 517.

23 Y. P. Kim, Y. H. Oh, E. Oh, S. Ko, M. K Han and H. SKim, *Anal. Chem.*, 2008, **80**, 4634.

24 X. Y. Cao, F. Shen, M. W. Zhang, J. J. Guo, Y. L. Luo, J. Y. Xu, Y. Li and C. Y. Sun, *Dyes and Pigments*, 2014, **111**, 99.

25 S. Pyne, G. P. Sahoo, D. K. Bhui, H. Bar, P. Sarkar, A. Maity and A. Misra, *Sens. Actuators B*, 2011, **160**, 1141.

26 L. Q. Guo, J. H. Zhong, J. M. Wu, F. F. Fu, G. N. Chen, Y. X. Chen, X. Y. Zheng and S. Lin, *Analyst*, 2011, 136, 1659.

27 M. Xue, X. Wang, H. Wang, D. Z. Chen and B. Tang, *Chem. Commun.*, 2011, **47**, 4986.

28 D. Bu, H. S. Zhuang, G. X. Yang and X. X. Ping, *Sens. Actuators B*, 2014, **195**, 540.

29 J. Song, F. Y. Wu, Y. Q.Wanand L. H. Ma, *Talanta*, 2015, **132**, 619.

30 K. C. Grabar, R. G. Freeman, M. B. Hommer and M. J. Natan, *Anal. Chem.*, 1995, **67**, 735.

31 H. C. Dai, Y. Shi, Y. L. Wang, Y. J. Sun, J. T. Hu, P. J. Ni and Z. Li, *Sens. Actuators B*, 2014, **202**, 201.

32 M. M. Maye, L. Han, N. N. Kariuki, N. K. Ly, W. B. Chan, J. Luo and C. J. Zhong, *Anal. Chim. Acta*, 2003, **496**, 17.

33 Y. P. Sun, B. Zhou, Y. Lin, W. Wang, K. A. S. Fernando and P. Pathak, *J. Am. Chem. Soc.*, 2006, **128**, 7756.

34 L. B. Tang, R. B. Ji, X. K. Cao, J. Y. Lin, H. X. Jiang and X. M. Li, *ACS Nano*, 2012, **6**, 5102.

35 K. Q. Qu, J. S. Wang, J. S. Ren and X. G. Qu, *Chem. Eur. J.*, 2013, **19**, 7243.

36 F. Gao, Q. Q. Ye, P. Cui and L. Zhang, *J. Agric. Food Chem.*, 2012, **60**, 4550.

37 K. G. Thomas, J. Zajicek and P. V. Kamat, *Langmuir*, 2002, **18**, 3722.

38 E. Oh, M. Y. Hong, D. Lee, S. H. Nam, H. C. Yoon and H. S. Kim, *J. Am. Chem. Soc.*, 2005, **127**, 3270.

39 A. Bahta, G. A. Parker and D. G. Tuck, *Pure Appl. Chem.*,1997, **69**,1489.

40 Y. J. Chen, L. Yao, Y. Deng, D. D. Pan, E. Ogabiela, J. X. Cao, S. B. Adeloju and W. Chen, *Microchim Acta*, 2015, **182**, 2147.

41 K. Tsuge, M. Kataoka and Y. Seto, *J. Health Sci.*, 2000, **46**, 343.

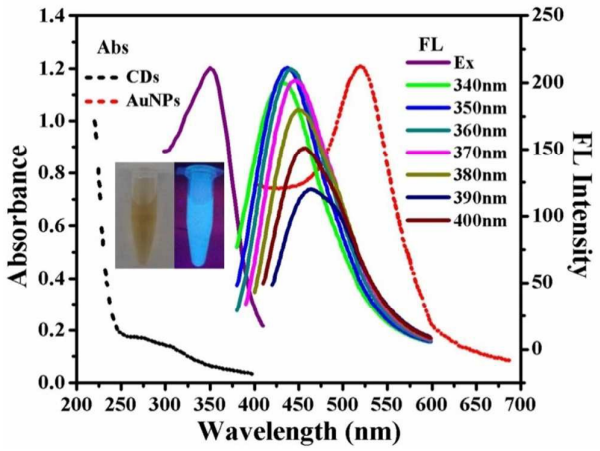

Fig. 1. The UV-vis absorption spectra of CDs and AuNPs; the excitation spectrum and emission spectra of CDs. Inset shows the photograph of the CDs under visible light (left) and 365 nm UV light (right), respectively.

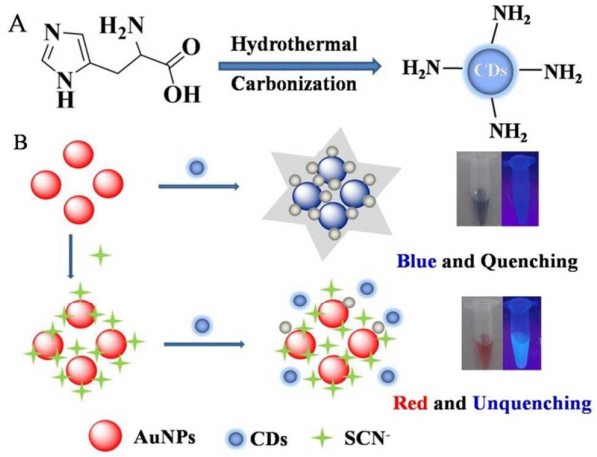

Scheme 1. The schematic illustration of (A) the synthetic process of amino-functionalized CDs and (B) the mechanism of the dual-readout nanosensor for SCN^- detection.

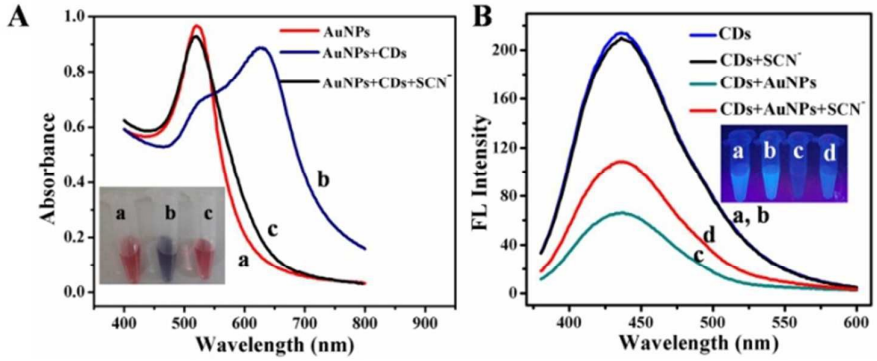

Fig. 2. (A) UV-vis absorption of AuNPs (a), AuNPs + CDs (b) and AuNPs + CDs+ SCN^- (c). (B) Fluorescence emission spectra of the CDs (a), CDs + SCN^- (b), CDs + AuNPs (c) and CDs + AuNPs + SCN^- (d). Inset shows the corresponding color changes.

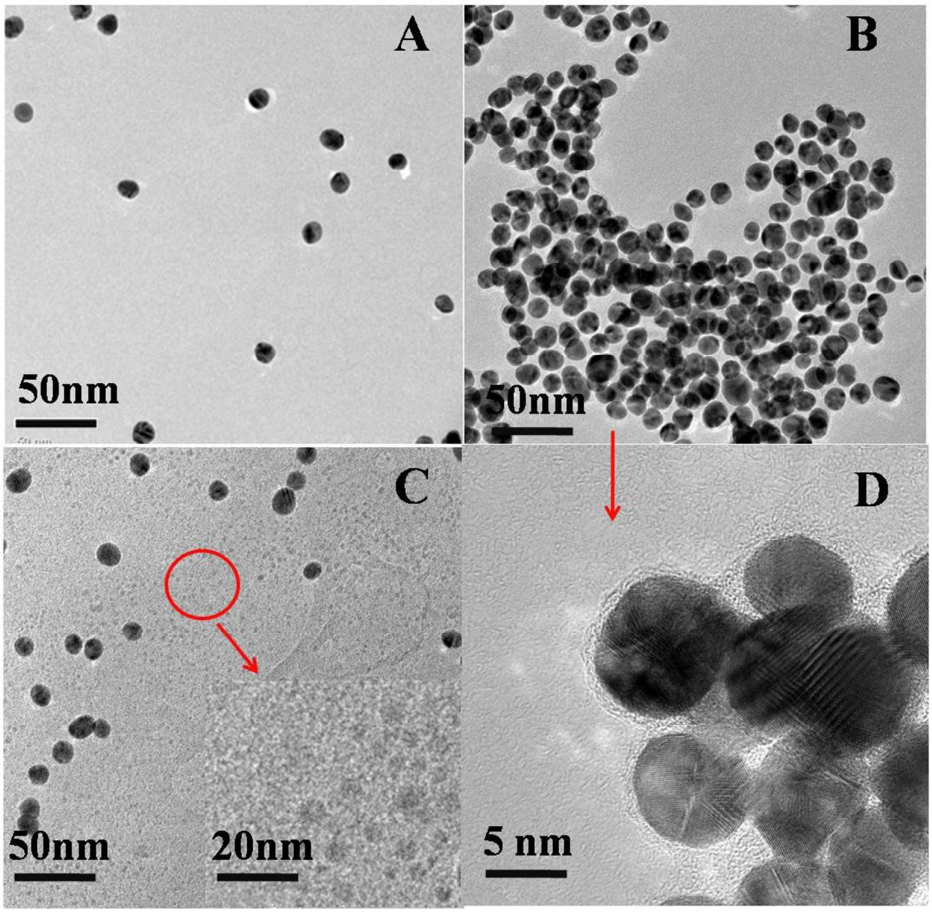

Fig. 3. TEM images of dispersed AuNPs (A), aggregated AuNPs induced by CDs in the absence of SCN^- (B), the dispersed AuNPs in the presence of CDs and SCN^- (C) and HRTEM image of aggregated AuNPs induced by CDs (D).

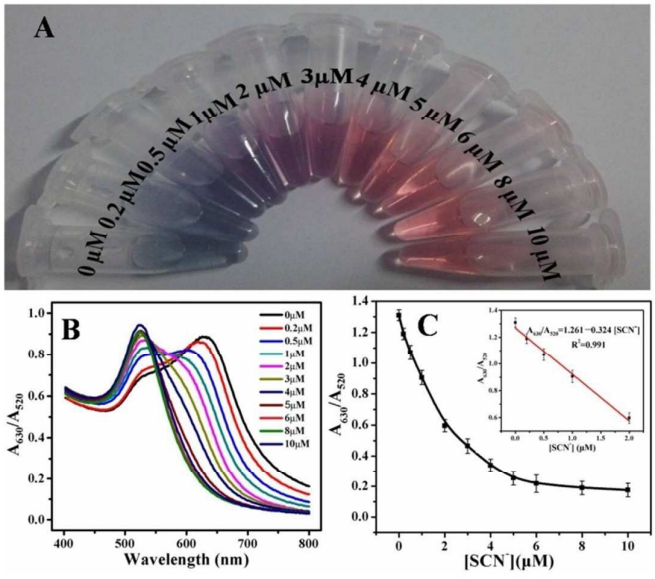

Fig. 4. (A) Photographs of colorimetric responses toward various concentrations of SCN^-. (B) UV-vis absorption spectra of the proposed assay in the presence of different amounts of SCN^-. (C) Relationship between the A_{630}/A_{520} ratio and the concentration of SCN^- (Inset shows the linear calibration plot corresponding to the SCN^- concentration).

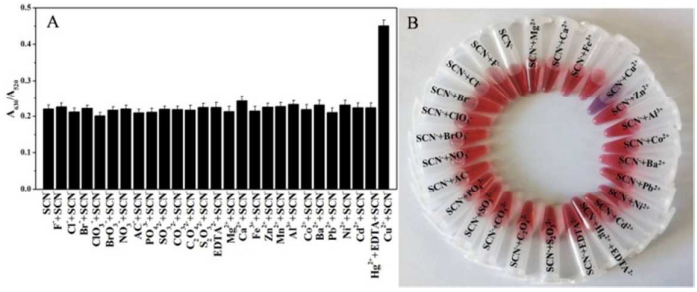

Fig. 5. (A) Interference study of the sensor in the presence of a mixture of SCN^- and another foreign ion. (B) shows the corresponding digital images. Concentrations: 5 μM for SCN^-, 10 μM for Br^- and Fe^{3+}, and 50 μM for other ions.

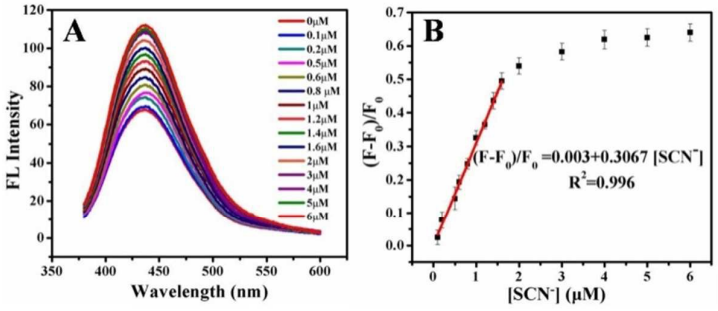

Fig. 6. (A) The fluorescence emission spectra of CDs in the presence of different concentrations of SCN^-. (B) The fluorescence enhancement efficiency as a function of SCN^- concentration.

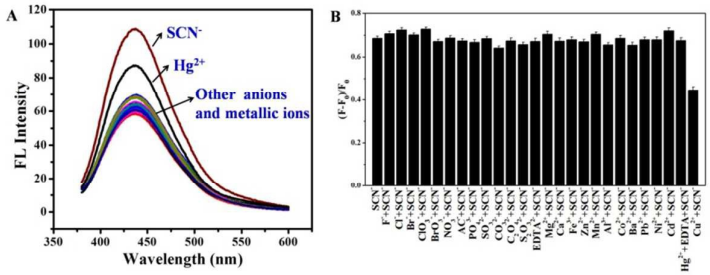

Fig. 7. (A) The fluorescence emission spectra of the proposed assay in the presence of SCN^- or other foreign anions and metallic ions. (B) Interference study of the sensor in the presence of a mixture of SCN^- and other foreign ion. Concentrations: 5 μM for SCN^-, 10 μM for Br^- and Fe^{3+}, and 50 μM for other ions.

Table 1. The application of the proposed nanosensor for determination of SCN^- in tap water and human saliva samples.

Samples	Measure Mode	Found in sapmles (μM)	Added (μM)	Total found (μM)	Recovery (%)	RSD (n=3, %)
Tap Water	Colorimetry	—	0.5	0.501	100.2	3.12
			1	0.897	89.7	2.98
			1.5	1.42	94.6	3.47
	Fluorimetry	—	0.5	0.489	97.8	2.64
			1	1.02	102	2.13
			1.5	1.45	96.6	2.97
Non-smoker	Colorimetry	0.546	1	1.56	101.4	2.65
saliva [a]	Fluorimetry	0.568	1	1.55	98.2	1.97
Smoker	Colorimetry	0.724	1	1.66	93.7	3.56
saliva [b]	Fluorimetry	0.743	1	1.75	100.7	2.39

[a] diluted by 200 times, [b] diluted by 1000 times.